

1 This is a preprint of the paper entitled "Grüneisen parameter formalism in the study of the Earth's  
2 core formation: a sensitivity study" by Vincent Clesi and Renaud Deguen. This version is the  
3 version that has been reviewed and accepted for publication in the journal Geophysical Journal  
4 International in March 2024. The proof reading and editing has not been done yet

# 5 **Grüneisen parameter formalism in the study of the Earth's** 6 **core formation: a sensitivity study**

7 Vincent Clesi<sup>1,2</sup> and Renaud Deguen<sup>3,1</sup>

<sup>1</sup> *Univ Lyon, ENSL, UCBL, UJM, CNRS, LGL-TPE, F-69007 Lyon, France*

<sup>2</sup> *Rice University Department of Earth Science. Keith-Wiess Geological Laboratory. 6100 Main Street Houston*

<sup>3</sup> *Univ. Grenoble Alpes, Univ. Savoie Mont Blanc, CNRS, IRD, Univ. Gustave Eiffel, ISTerre, 38000 Grenoble, France*

## 8 **SUMMARY**

9 The Grüneisen parameter is an important parameter for the thermal state and evolution of the  
10 core, but its uncertainties and their implications are sometimes overlooked. Several formalisms  
11 using different parameters values have been used in different studies, making comparison be-  
12 tween studies difficult. In this paper, we use previously published datasets to test the sensitivity  
13 of modeling the thermal state of the early core to the different formalisms and parameter val-  
14 ues used to describe the evolution of the Grüneisen parameter with density. The temperature of  
15 the core obtained in our models is less sensitive to the uncertainties of the parameters used in  
16 Al'Tshuler et al. (1987) formalism than the uncertainties of the parameters used in Anderson  
17 (1967) formalism.

18 **Key words:** Composition and structure of the core – Planetary interiors – Numerical mod-  
19 elling – High-pressure behaviour– Equations of state.

## 20 **1 INTRODUCTION**

21 Constraining the core heat content, whether at the present time (Lin et al. 2003; Labrosse 2015) or  
22 for the primitive core (Clesi & Deguen 2023), implies making assumptions on the thermal expan-

23 sion and compressibility of the core components. For this, the Grüneisen parameter (first defined in  
24 Grüneisen 1912) is often used. This parameter has the advantage of being comprised between 0.9  
25 and 2 for metallic materials, which is a narrower range than the thermal expansion coefficient or  
26 bulk modulus, and its value has been determined by different methods : thermodynamical model-  
27 ing (Anderson 1967; Al'Tshuler et al. 1987), ab initio (Dubrovinsky et al. 2000; Alfè et al. 2007),  
28 experiments (Jeanloz 1979; Umemoto & Hirose 2015). Using the Grüneisen parameter allows to  
29 simplify the models by getting rid of the thermal expansion parameter  $\alpha$  which is more sensitive  
30 to the composition.

31 However, there are several approaches to model the variations of the Grüneisen parameter, es-  
32 pecially with pressure. Some studies assume a constant value (Anderson & Ahrens 1994; Labrosse  
33 2015), some use the Al'Tshulher formalism (Al'Tshuler et al. 1987; Dewaele et al. 2006; Umem-  
34 oto & Hirose 2015), some use the power law first proposed by Anderson in 1967 (Anderson 1967;  
35 Dubrovinsky et al. 2000; Kuwayama et al. 2020), while others calculate it within the study: by ab  
36 initio in Alfè et al. (2007) and Ichikawa et al. (2014), by linear expansion in Badro et al. (2014). In  
37 this paper, we will use the results of our previous study (Clesi & Deguen 2023) to assess the model  
38 sensitivity to different approaches of Grüneisen parameter when modeling the initial heat content  
39 of the core. We use previous results linking core composition and temperature, and test different  
40 ways of calculating the value of  $\gamma$ . By fitting the effect of each parameter on temperature, we can  
41 assess the variations introduced by using different formalisms, and the error introduced by varia-  
42 tions of the parameters within the formalism chosen. We show that the formalism of Al'Tshuler  
43 (Al'Tshuler et al. 1987) is less prone to yield large errors in the calculations while being theoretic-  
44 ally the most sound of all formalism studied.

## 45 **2 GRÜNEISEN PARAMETER MODELING AND THERMAL MODEL**

### 46 **2.1 Accretion scenario and thermal modeling**

47 We use the accretion and core/mantle differentiation models that have been previously determined  
48 in Clesi & Deguen (2023). These models yield mantle compositions close to the Bulk Silicate Earth  
49 (BSE) given in McDonough & Sun (1995), while yielding compositions for the core compatible

50 with a  $\sim 10\%$  wt. of light elements (Si and O) in the core. To determine the heat content and  
51 temperature of the core we consider the following steps :

52 (i) The initial temperature of each addition of metal is set at the bottom of the magma ocean,  
53 where the metal is assumed to equilibrate with the silicates. The initial temperature is therefore  
54 given by the liquidus of silicate at the pressure of the bottom of the magma ocean, as given by  
55 Andraut et al. (2011).

56 (ii) The metal is then heated by compression while migrating from the bottom of the magma  
57 ocean to the growing core. At each step of accretion its composition is different, and we do not  
58 consider any mixing, thus resulting in the formation of a stratified core (as in Jacobson et al.  
59 (2017))

60 (iii) The initial temperature profile is then set by the additional compression of the metal up to  
61 the final core pressures. We use this initial temperature and density profile to calculate the heat  
62 content.

63 (iv) We assume that the core is then mixed from the stratified state to an isentropic state, and use  
64 the previously calculated heat content to get the corresponding temperature at the CMB ( $T_{CMB}^{is}$ ).  
65 This is a strong assumption, since the core is often found to be stably stratified at the end of accre-  
66 tion (Clesi & Deguen 2023). Whether the core would be efficiently mixed depends on the radial  
67 variations in composition, ratio of temperature gradient to isentropic gradient (which depends on  
68  $\gamma$ ), and of the nature and intensity of the possible stirring processes (Jacobson et al. 2017; Bouffard  
69 et al. 2020). However, the main purpose of this assumption is to provide a single measure of the  
70 temperature of the core – the temperature  $T_{CMB}^{is}$  of the CMB after mixing to an isentropic state –  
71 which can be seen as a convenient measure of the amount of heat stored into the core.

72 The details on the model and the different calculations are described in Clesi & Deguen (2023).  
73 The main result of the paper is that mean pressure of metal-silicate equilibrium, light elements  
74 concentration in the core, and core temperature are positively correlated. A summary of the results  
75 are presented in Figure 1.

76 The initial temperature of the metal is set to be the liquidus temperature of the silicate (Andraut

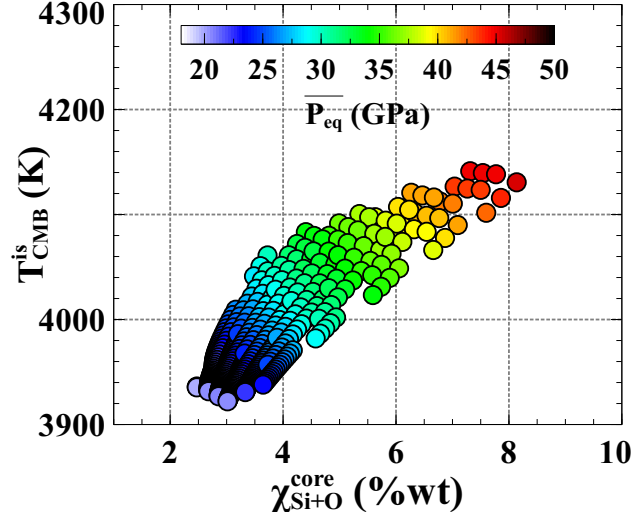


**Figure 1.** Summary of the results from Clesi & Deguen (2023), showing the correlation between the isentropic temperature at the CMB at the end of accretion (y-axis), light elements concentration in the core (here Si and O, x-axis) and mean value of equilibrium pressure ( $\overline{P_{eq}}$ , color scale). The temperatures obtained here are obtained with the Grüneisen parameter calculated with Al'Tshuler formalism, with  $\gamma_0 = 1.875$  and  $\gamma_\infty = 1.305$ . The points plotted here are the models matching the compositional constraints defined in Clesi & Deguen (2023).

et al. 2011) at the bottom of the magma ocean where chemical equilibrium happens. It is given by:

$$T_{eq} = 1940 \left( \frac{P_{eq}}{29} + 1 \right)^{1/1.9}. \quad (1)$$

where  $P_{eq}$  is the pressure at the bottom of the magma ocean (in GPa) which is the pressure where metal and silicate are equilibrated. The temperature changes calculated in steps (ii) and (iii) are obtained from:

$$\frac{dT}{dP} = \frac{\gamma T}{K_s}. \quad (2)$$

where  $\gamma$  is the Grüneisen parameter of the metal,  $T$  its temperature and  $K_s$  its isentropic bulk modulus. We use the Murnaghan approximation for the bulk modulus,

$$K_s = K_0 + K'P, \quad (3)$$

with  $K_0 = 128.49$  GPa the bulk modulus for  $P=0$ , and  $K' = 3.67$  the first derivative of the bulk modulus, which yields the following equation of state for the metal:

$$\frac{\rho(P)}{\rho_0} = \left( 1 + \frac{K'}{K_0}P \right)^{1/K'}. \quad (4)$$

85 with  $\rho(P)$  is the density of the metal at pressure P. The value of  $\rho_0$ , i.e. the density of the metal  
 86 at the reference pressure, is varying throughout accretion, depending on the composition of the  
 87 metal, which is set by chemical equilibration with the silicates at the bottom of the magma ocean  
 88 (see Clesi & Deguen (2023) for the details).

89 The heat content of the core is then calculated as

$$Q = 4\pi \int_0^{R_c} \rho(r) C_p T(r) r^2 dr, \quad (5)$$

90 with  $R_C = 3470$  km the total radius of the core,  $C_p = 1000 J.kg^{-1}.K^{-1}$  the specific heat of the  
 91 metal and  $T(r)$  the temperature in the core at the radius r; where the distance  $r$  from the center  
 92 and the pressure are linked by

$$P_{core}(r) = P_{center} + \left( \frac{P_{CMB} - P_{center}}{R_c^2} \right) r^2 \quad (6)$$

93 with  $P_{CMB}$  and  $P_{center}$  the pressure at the CMB and at the center of the core, respectively. The  
 94 isentropic temperature profile can then be obtained from

$$\left( \frac{\partial \ln T^{is}}{\partial \ln \rho^{is}} \right)_s = \gamma. \quad (7)$$

95 where  $\rho^{is}$  is the density profile of the core after isentropic mixing. As seen in Equation 7, the final  
 96 isentropic temperature is a function of the Grüneisen parameter,  $\gamma$ . Depending on the  $\gamma$  formalism  
 97 (constant value, Al'Tshuler et al. (1987) or Anderson (1967) power laws), integration of Equation  
 98 7 will yield different results. We then consider that the core is fully mixed with a constant heat  
 99 content. The isentropic mixed core temperature profile is determined by integration of Equation 7  
 100 for a mixed density profile  $\rho^{is}(r)$ , and combined with the heat content calculated by Equation 5,  
 101 we can calculate the temperature at the CMB after mixing as

$$T_{CMB}^{is} = \frac{Q}{4\pi \int_0^{R_c} \rho^{is}(r) C_p T^{is}(r) r^2 dr}, \quad (8)$$

102 which is evaluated numerically. In the following sections, we calculate  $T_{CMB}^{is}$  from equation 8  
 103 for the three different formalisms tested in this study, and we vary parameters values within each  
 104 of the formalism to determine the sensitivity of  $T_{CMB}^{is}$  to the formalisms and parameter values.  
 105 Before varying the parameters, Figure 2 shows how, for three solutions in the dataset presented  
 106 in Figure 1, changing the formalism affects each step of the calculation. As can be seen on this

107 figure, changing the value of the Grüneisen parameter tends to shift the temperature profiles up  
 108 and down, irrespectively of the stratification.

## 109 **2.2 Constant gruneisen parameter**

110 The first assumption that can be made is assuming  $\gamma$  to be constant. Integration of Equation 2 then  
 111 yields:

$$T(P) = T_{eq} \left( \frac{K'P + K_0}{K'P_{eq} + K_0} \right)^{\frac{\gamma}{K'}}. \quad (9)$$

112 This equation is used as input to calculate the heat content (Equation 5) and then the value of  
 113  $T_{CMB}^{is}$  (Equation 8).

## 114 **2.3 Power law formalism of Anderson**

115 The second assumption is that the variation of  $\gamma$  follows a power law of the form

$$\gamma = \gamma_0 \left( \frac{\rho_0}{\rho} \right)^b. \quad (10)$$

116 where  $\gamma_0$  is the Grüneisen parameter for  $\rho = \rho_0$  and  $b$  is the exponent of the power law. This  
 117 formalism has been proposed by Anderson (1967), in order to simplify the calculation of the  
 118 thermal expansion coefficient of some materials. This power law is practical for integration, and  
 119 is especially fitted for Murnaghan equation of state, as it was one of the reasons for choosing  
 120 this formalism in the original paper. Equation 2 with  $\gamma$  given by (10) has the following analytical  
 121 solution:

$$T(P) = T_{eq} \exp \left[ \frac{\gamma_0}{b} \left( \left( 1 + \frac{K'P_{eq}}{K_0} \right)^{-b/K'} - \left( 1 + \frac{K'P}{K_0} \right)^{-b/K'} \right) \right]. \quad (11)$$

## 122 **2.4 Formalism of Al'Tshuler**

123 The last model investigated in this study is given by

$$\gamma = \gamma_\infty + (\gamma_{0,j} - \gamma_\infty) \left( \frac{\rho_0}{\rho} \right)^\beta, \quad (12)$$

124 where  $\beta = \gamma_{0,j}/(\gamma_{0,j} - \gamma_\infty)$ , and  $\gamma_{0,j}$  the Grüneisen parameter for  $\rho = \rho_0$  and  $\gamma_\infty$  the asymptotic  
 125 value of the Grüneisen parameter when  $P \rightarrow \infty$ . This equation also takes the form of a power

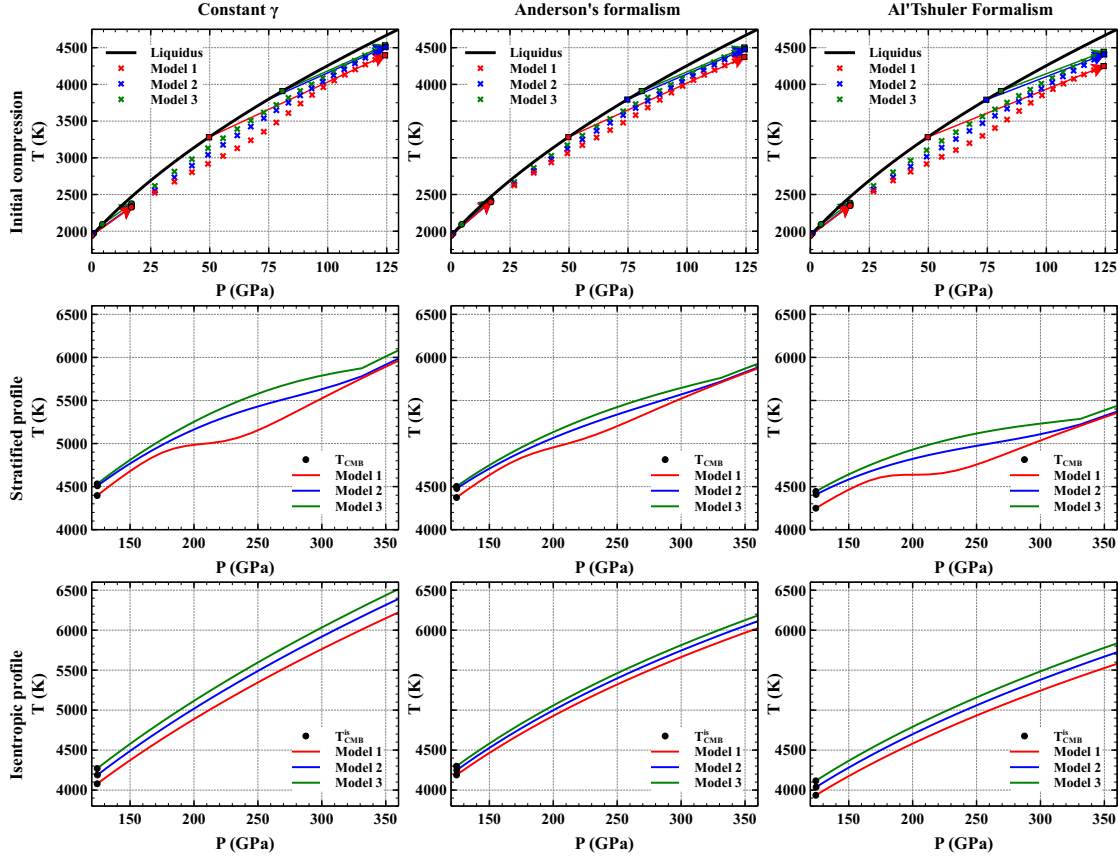


**Figure 2.** Description of three steps of the model for different formalisms of the Grüneisen parameter tested in this study. Left column: constant  $\gamma = 1.7$ . Middle column: Anderson's power law, with  $\gamma_0 = 2.05$  and  $b = 0.6$ . Right column: Al'Tshuler formalism with  $\gamma_0 = 1.305$  and  $\gamma_\infty = 1.875$ . Each row represents one of the steps of the scenario described in section 2.1. Top row: initial compression between the bottom of the magma ocean and the growing core-mantle boundary (step (i) and part of step (ii) in the text), with the liquidus curve in black and the adiabat of the first and last steps of the model shown by the arrows. The cross symbols represents the P-T conditions of the metal reaching the CMB at each step of accretion, before the core is fully formed. The arrows show the changes in P-T conditions undergone by the metal through the crystallized part of the mantle in the first step of accretion (round markers) and last step of accretion (square markers). Middle row: temperature profile of the core when stratified and after compression of the metal due to the growth of the core (step (ii) and step (iii) in the text). Bottom row: temperature profile in the core after mixing to an isentropic state (step (iv) in the text). The black dots mark the temperature at the CMB. A similar figure with more details on the model steps can be found at Clesi & Deguen (2023). Red curves: Model 1, obtained for the  $f_c = 0.6$ ,  $a_P = 0.4$  and  $\lambda = 5$ , with  $\overline{P_{eq}} = 19.7$  GPa and  $\chi_{Si+O}^{core} = 2.47\%$ . Blue curves: Model 2, obtained for the  $f_c = 0.85$ ,  $a_P = 0.6$  and  $\lambda = 1$ , with  $\overline{P_{eq}} = 34.1$  GPa and  $\chi_{Si+O}^{core} = 5.24\%$ . Green curves: Model 3, obtained for the  $f_c = 1$ ,  $a_P = 0.65$  and  $\lambda = 0.4$ , with  $\overline{P_{eq}} = 43.9$  GPa and  $\chi_{Si+O}^{core} = 7.86\%$ .

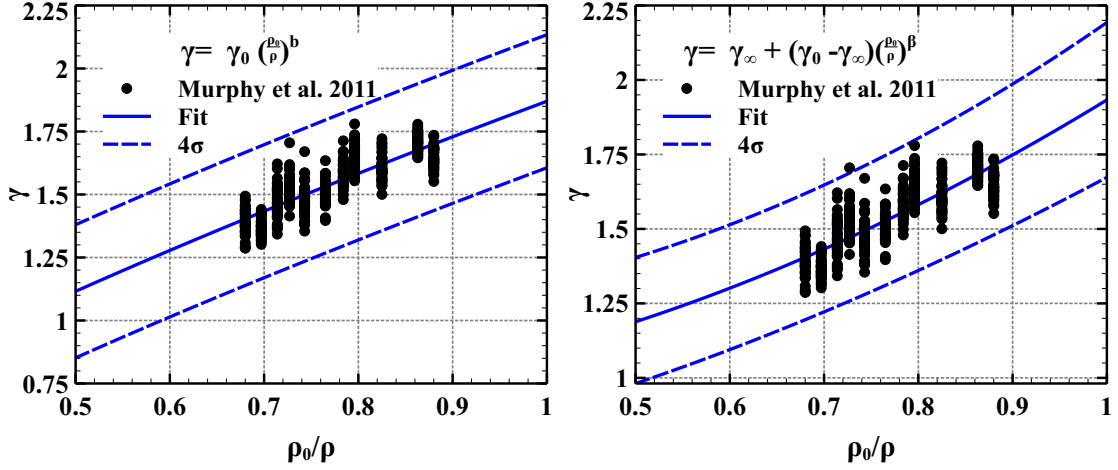


**Figure 3.** Results of the fit from the data of Murphy et al. (2011) with the formalism of Anderson (1967) (left panel) and Al’Tshuler et al. (1987) (right panel). The data from Murphy et al. (2011) have been bootstrapped to account for the error bar by randomly distributing 20 values for each point following a gaussian distribution, thus allowing the fit to be made on  $\sim 200$  points instead of 10.

126 law, used by multiple studies (Dewaele et al. 2006; Clesi & Deguen 2023). It is however different  
 127 than the one from Anderson (1967), because it is derived from the theoretical isothermal density  
 128 evolution of metal (Al’Tshuler et al. 1987). Though equation 12 might be seen as an extended  
 129 version of Anderson’s power law (it is the sum of a power law in  $\rho$  and a constant), note that the  
 130 power exponent and the prefactor of the power law part are here linked theoretically, which is  
 131 not the case in Anderson’s power law. One implication is that the number of parameters involved  
 132 in Al’Tshuler’s formalism is not higher than in Anderson’s formalism, in spite of its seemingly  
 133 greater complexity. With this formalism, integrating equation 2 gives

$$\begin{aligned}
 T(P) &= T_{eq} \left( \frac{K_0 + K'P}{K_0 + K'P_{eq}} \right)^{\frac{\gamma_\infty}{K'}} \\
 &\times \exp \left[ \frac{\gamma_{0,j} - \gamma_\infty}{\beta} \left( \left( 1 + \frac{K'P_{eq}}{K_0} \right)^{-\frac{\beta}{K'}} - \left( 1 + \frac{K'P}{K_0} \right)^{-\frac{\beta}{K'}} \right) \right].
 \end{aligned} \tag{13}$$

## 134 2.5 Sensitivities of $T_{CMB}^{is}$ to the different parameters

135 In order to compare the three formalisms presented above, we fitted equations (10) and (12) to  
 136 a dataset of Grüneisen parameter measurements for pure iron. This allows to obtain in a self-  
 137 consistent way the values and uncertainties of the parameters appearing in Al’Tshuler et al. (1987)  
 138 and Anderson (1967)’s formalisms. We use the dataset provided by Murphy et al. (2011), to which

Parameters	$\gamma_0$	$b$	$\gamma_{0,j}$	$\gamma_\infty$
Mean value	1.875	0.752	1.933	0.916
Minimum value	1.555	0.432	1.608	0.591
Maximum value	2.195	1.07	2.258	1.241
$1\sigma$	0.08	0.08	0.0812	0.0812

**Table 1.** Values obtained from fitting the measurements of  $\gamma$  from Murphy et al. (2011) to the Anderson's and Al'Tshuler's formalisms.

we fitted the values of  $\gamma_0$ ,  $b$ ,  $\gamma_\infty$  and  $\gamma_{0,j}$  (Figure 3). Given the limited number of points (10) in the dataset, we created for each value of  $\frac{\rho_0}{\rho}$  a random dataset of 20  $\gamma$  values distributed following a normal law centered on the mean value with a standard deviation equal to the uncertainty given in Murphy et al. (2011). We then fitted the parameters of each formalism to the dataset, thus allowing us to define a range of value for each parameter, given in Table 1, that will be tested throughout the study.

We use the subset of core formation models ( $n = 382$ ) from Clesi & Deguen (2023). Each solution represents a different evolution of the core composition while yielding an acceptable fit on the Bulk Silicate Earth (McDonough & Sun 1995). We then calculate for each solution the CMB temperature after core mixing with equations 5 and 8 with the three different formalisms: equation 9 for constant  $\gamma$ , equation 10 for Anderson's power law, and equation 13 for Al'Tshuler's formalism. We vary each parameter independently to assess their effect on the mean and variance of  $T_{CMB}^{is}$  value on the 382 models tested. In the following sections we discuss the strengths and weaknesses of each formalism in the same style.

For each formalism, we estimate the effect of varying parameter values on the mean value of  $T_{CMB}^{is}$  in the dataset. In order to estimate the sensitivity of the model results to the parameters, we fitted a linear equation to explain the mean  $T_{is}^{CMB}$  value of our dataset:

$$T_{CMB}^{is} = a_0 + a_1x \quad (14)$$

where  $x$  is one of the parameters ( $\gamma$ ,  $\gamma_0$ ,  $b$  or  $\gamma_\infty$ ).

The size of the dataset we chose (382 different accretion scenarios, spanning different core

158 compositions, see Clesi & Deguen (2023)) also allows us to assess the sensitivity of the actual  
 159 values within a formalism to the others parameters in the models. Indeed, the variations of  $T_{CMB}^{is}$ ,  
 160 as shown in Clesi & Deguen (2023), depend also on the composition of the core (light element  
 161 concentrations), the pressure of equilibrium and its variation throughout accretion as well as the  
 162 oxygen fugacity of the impactors. A small dispersion of the  $T_{CMB}^{is}$  values means that the Grüneisen  
 163 parameter obtained for the set of parameter tends to mask the sensitivity of the model to other  
 164 parameters (composition, pressure...). A large dispersion of  $T_{CMB}^{is}$  on the other hand means that  
 165 the Grüneisen parameter tend to exacerbate the effect of the other parameters of the model.

166 As shown in the following sections, varying the values of the Grüneisen parameter can change  
 167 the output of the same models by several hundreds of Kelvin. When modeling the compression  
 168 of liquid metal, especially at high pressure, the data on compressibility is mostly derived from  
 169 solid iron experiments and *ab initio* calculations. This situation presents several problems when  
 170 modeling the Earth's core: the fact that liquid metal compressibility is not well constrained, and  
 171 the fact that several light elements can affect this compressibility compared to pure iron. The  
 172 Grüneisen parameter presents the advantage of having a limited range of value, thus extrapolating  
 173 from solid iron value to the metal alloy forming the core limits the risk in terms of temperature  
 174 calculation.

175 On the other hand, this advantage of having less chance to be far away from the results can  
 176 become a disadvantage when trying to be more precise (for instance investigating the effect of  
 177 small variations in composition on the temperature).

178 In the following sections we discuss the effect and robustness of the different formalisms pre-  
 179 sented above by using the sensitivity results obtained by fitting Equation 14 to the mean values  
 180 of  $T_{CMB}^{is}$ . To do so we will estimate the variation of temperature induced by a deviation from the  
 181 following values:

- 182 - in Section 3, a constant  $\gamma$  of 1.7, as used by Labrosse (2015) ;
- 183 - in section 4, Anderson (1967) formalism with  $\gamma_0 = 2.05$  and  $b = 0.63$  from Kuwayama et al.  
 184 (2020);

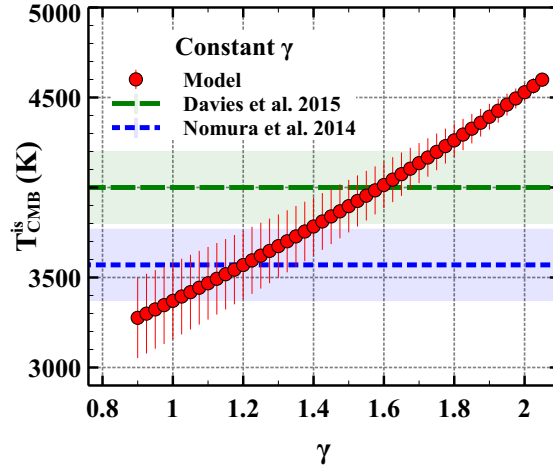


**Figure 4.** Variation of the mean  $T_{CMB}^{is}$  determined by Equations 8 and 9 as a function of  $\gamma$ . The error bar are the  $2\sigma$  variation on the subset of core formation models used in this study. For comparison the estimates of current CMB temperature from Nomura et al. (2014) (dotted blue line) and Davies et al. (2015) (dashed green line) are also shown.

185 - in Section 5, Al'Tshuler et al. (1987) formalism with  $\gamma_0 = 1.875$  and  $\gamma_\infty = 1.305$  from Clesi  
 186 & Deguen (2023).

### 187 3 CONSTANT GAMMA

188 Figure 4 shows the effect of varying the value of a constant  $\gamma$  on the isentropic temperature at the  
 189 CMB. The range of  $\gamma$  tested is between 0.9 and 2.1, which is representative of the range of values  
 190 of  $\gamma$  for iron given by several authors (see Dubrovinsky et al. (2000) or Wagle & Steinle-Neumann  
 191 (2019) and references therein).  $T_{CMB}^{is}$  is increasing with increasing  $\gamma$ : the mean value goes from  
 192 3424 K to 4615 K. The effect of  $\gamma$  on the mean CMB temperature can be fitted by a polynomial  
 193 function, for which the parameters are given in Table 2.

194 The  $2\sigma$  values are higher as  $\gamma$  decreases: from 440 K at  $\gamma = 0.9$  to 60 K at  $\gamma = 2.05$ . This

$a_0$	$a_1$	$\chi^2$
2116	1202	1.6676

**Table 2.** Values of parameters fitting the trend of mean values in Figure 4. The equation fitted is Equation 14 with  $x$  replaced by  $\gamma$ .

indicates that the variability coming from the different accretion histories is buffered by high values of  $\gamma$ .

From Table 2, it is possible to calculate the  $\Delta T$  (error on the final temperature at the CMB) induced by changing the value of  $\gamma$  from a reference value chosen to be  $\gamma = 1.7$ . With the value of  $a_1$  from Table 2, changing  $\gamma$  by  $\pm 0.1$  induces a variation  $\Delta T = 120$  K, which is higher than the dispersion of values observed in the other formalisms tested in this study. This trend shows that the results are highly sensitive to the value of a constant  $\gamma$ .

#### 4 ANDERSON'S POWER LAW

The formalism of Anderson (1967) has two parameters that can affect the sensitivity of  $T_{CMB}^{is}$  to  $\gamma$ . The parameter  $b$  values are empirically fitted for each composition of the metal, with values spanning from 0.63 (Kuwayama et al. 2020) and 0.69 (Dubrovinsky et al. 2000) to 1.0 (McQueen et al. 1970) and 1.69 (Jeanloz 1979). In the case of liquid metal, most of the values converges toward  $b \leq 1$ . Here we tested values of  $b$  between 0.4 and 1.1 so as to cover the entire range of  $b$  values obtained from the fitting of Murphy et al. (2011)'s data set (see Table 1). As for the  $\gamma_0$  value, it is the value for liquid metal at 1 bar, and since  $\gamma$  decreases with pressure it has to be higher than the value of  $\gamma$  at high pressures. The published range for  $\gamma_0$  is between 1.59 (Brown & McQueen 1986) and 2.05 (Kuwayama et al. 2020), with 1.713 (Anderson & Ahrens 1994) and 1.8 (Dubrovinsky et al. 2000) having also been proposed and used. As for the value of  $b$ , we tested the range presented in Table 1, which is 1.5 to 2.2.

The top panel of Figure 5 shows that increasing the value of  $\gamma_0$  tends to increase the mean value of  $T_{CMB}^{is}$ , irrespectively of the value of  $b$ . For  $\gamma_0 = 1.2$ , the mean value of  $T_{CMB}^{is}$  is between 3227 K and 3492 K, and for  $\gamma_0 = 2.1$  the mean value is between 3869 K and 4474 K, depending on the value of  $b$ ; for  $b = 1.1$ , the temperature varies between 4131 and 3500 K over the same  $\gamma_0$  range. The sensitivity of  $T_{CMB}^{is}$  to  $\gamma_0$  is stronger at the lower values of  $b$ , though this effect is not very strong. The bottom panel of Figure 5 shows the effect of increasing the exponent of the power law. The higher  $b$  is, the lower the temperature is: for  $b = 0.4$  the temperature is between 4535 K and 3750 K depending on  $\gamma_0$  values; for  $b = 1.1$  the mean value is between 3527 K and

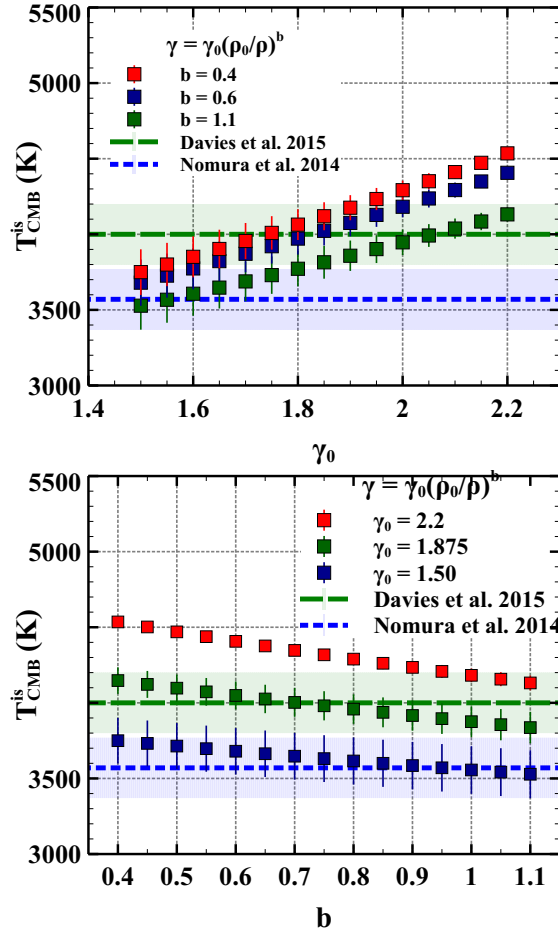


**Figure 5.** Top Panel: Effect of  $\gamma_0$  on  $T_{CMB}^{is}$  for different values of  $b$ . Red squares:  $b = 0.4$ . Dark blue squares:  $b = 0.6$ . Dark green squares:  $b = 1.1$ .

Bottom panel: Effect of  $b$  on  $T_{CMB}^{is}$  for different values of  $\gamma_0$ . Red squares:  $\gamma_0 = 2.2$ . Dark green squares:  $\gamma_0 = 1.875$ . Dark blue squares:  $\gamma_0 = 1.5$ .

$T_{CMB}^{is}$  is calculated from equations 8 and 11. For comparison, we also show the estimates of present-day CMB temperature from Nomura et al (2014) (dotted blue line, lower estimate) and the review of Davies et al. (2015) (dashed green line).

222 4131 K. The higher the value of  $\gamma_0$  and the lower the value of  $b$ , the lower the dispersion of values:

223 for  $b = 0.4$ , the  $2\sigma$  variation is 22 K at  $\gamma_0 = 2.2$  and 150 K at  $\gamma_0 = 1.5$ ; for  $b = 1.1$  the  $2\sigma$  is 48 K

224 and 160 K for  $\gamma_0 = 2.2$  and  $\gamma_0 = 1.5$  respectively.

225 A linear fit (Equation 14) of the effect of both parameters on the mean values can be performed  
 226 with good  $\chi^2$  values. The fitted parameter are shown in Table 3, showing a positive effect of  $\gamma_0$ ,  
 227 and a negative effect of  $b$ .

228 Let us now assume that we used the values of  $\gamma_0 = 2.05$  and  $b = 0.6$  from Kuwayama et al.

Conditions	$a_0$	$a_1$	$\chi^2$
$b = 0.4$	1984	1158	0.1855
$b = 0.6$	2059	1065	0.1151
$b = 1.1$	2197	877	0.0424
$\gamma_0 = 2.2$	4764	-587	0.4068
$\gamma_0 = 1.875$	4319	-445	0.0244
$\gamma_0 = 1.5$	3872	-317	0.0041

**Table 3.** Values of parameter fitting the trend of mean values in Figure 5. The equations fitted are:  $\overline{T_{CMB}^{is}} = a_0 + a_0\gamma_0$ , and  $\overline{T_{CMB}^{is}} = a_0 + a_1b$ . The first part of the table shows the variation for fixed values of  $b$  (Figure 5 left panel), and the second part shows the variation for fixed values of  $\gamma_0$  (Figure 5 right panel).

(2020) to make the calculation on the models of Clesi & Deguen (2023). It is then possible to use the parameters from table 3 to calculate what is the induced error if the 'true' values are different. For  $\gamma_0 = 2.2$ , changing  $b$  by only 0.1 (corresponding to 15% of the range of values given in Table 1) changes  $T_{CMB}^{is}$  by 58 K. If we rather consider  $b = 0.6$ , then a variation of 0.1 (also corresponding to 15% of the range of values given in Table 1) for the parameter  $\gamma_0$  yields  $\Delta T \sim 100$  K.

The error induced by getting a wrong value for the exponent is therefore less important than getting the value of  $\gamma_0$  wrong, but the variations are not negligible, especially if both parameters estimations are wrong: if for example  $\gamma_0 = 1.875$  and  $b = 0.4$ , then the final temperature calculated with the reference values ( $\gamma_0 = 2.05$  and  $b = 0.6$ ) is overestimated by  $\sim 300$  K.

## 5 AL'TSHULER POWER LAW

The formalism of Al'Tshuler et al. (1987) depends on two parameters,  $\gamma_0$  and  $\gamma_\infty$ , with  $\gamma_\infty < \gamma_0$ . The values of  $\gamma_\infty$  represent the minimum value of the Grüneisen parameter for infinite pressure (i.e. when the compressibility reaches a minimum asymptotic value) due to the quantum-statistical Grüneisen coefficient under extreme pressure (Gilvarry 1956; Burakovsky & Preston 2004). For liquid iron this value is between 1 and 1.4 (Dewaele et al. (2006), and references therein), and we tested values between 0.6 and 1.25 as given in Table 1. As for  $\gamma_0$ , it is the value of the Grüneisen parameter at the pressure of the reference state ( $\rho/\rho_0 = 1$ ). Therefore it is higher than  $\gamma_\infty$  and

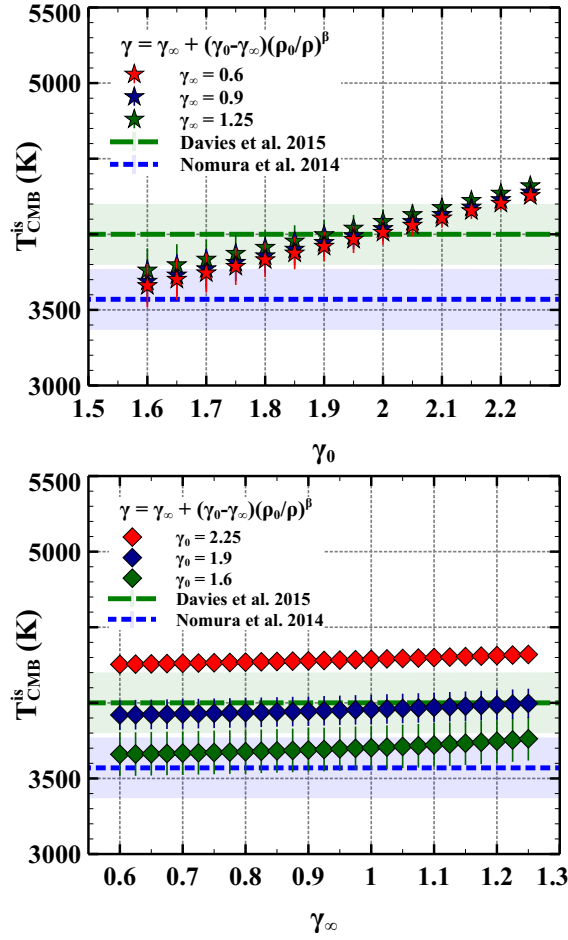


**Figure 6.** Evolution of the mean value of  $T_{CMB}^{is}$  as a function of  $\gamma_0$  (top) and  $\gamma_\infty$  (bottom) in the formalism of Al'Tshuler et al. (1987), given by equations 13 and 8. On the top panel  $\gamma_\infty$  values are fixed at 1, 1.25, 1.305 and 1.5. On the bottom panel,  $\gamma_0$  values are fixed at 2.05, 1.875, 1.75 and 1.5. For comparison we also show the estimates of current CMB temperature from Nomura et al. (2014) (dotted blue line) and Davies et al. (2015) (dashed green line).

246 close to the values of the parameter  $\gamma_0$  from Anderson (1967), studied in the previous section.  
 247 Here we tested values between 1.6 and 2.25, as given by the results of the fit in Table 1. Figure 6  
 248 shows that the temperature is positively correlated with both  $\gamma_0$  and  $\gamma_\infty$ . Higher values of  $\gamma_0$  lead  
 249 to less dispersion of the results: for instance, at  $\gamma_\infty = 0.6$ , the  $2\sigma$  value for the dataset is 35 K for  
 250  $\gamma_0 = 2.25$  and 144 K for  $\gamma_0 = 1.6$ . When  $\gamma_0$  is fixed, varying the value of  $\gamma_\infty$  has less impact on  
 251 the dispersion of the results: for instance at  $\gamma_0 = 1.6$ , the  $2\sigma$  for the dataset is 141 K for  $\gamma_\infty = 0.9$   
 252 and 128 K for  $\gamma_\infty = 1.25$ .

253 The variation of the mean temperature of our dataset is more affected by varying  $\gamma_0$  than  $\gamma_\infty$ .  
 254 For instance, the mean temperature goes from 4319 K to 3762 K with  $\gamma_\infty = 1.25$  and for  $\gamma_0$

Conditions	$a_0$	$a_1$	$\chi^2$
$\gamma_0 = 2.25$	4191	100	0.0047
$\gamma_0 = 1.9$	3845	115	0.0013
$\gamma_0 = 1.6$	3560	150	0.0020
$\gamma_\infty = 0.6$	2151	933	0.0538
$\gamma_\infty = 0.9$	2188	927	0.0629
$\gamma_\infty = 1.25$	2312	890	0.1284

**Table 4.** Values of parameters fitting the trend of mean values in Figure 6. The equation fitted is:  $\overline{T_{CMB}^{is}} = a_0 + a_1\gamma_x$ , with  $\gamma_x$  being  $\gamma_0$  or  $\gamma_\infty$ . The first part of the table are for fixed values of  $\gamma_\infty$ , the second one for fixed values of  $\gamma_0$ . The value of  $\chi^2$  for each fit is given in the last column.

255 varying from 2.25 to 1.6, respectively. On the other hand the temperature decreases from 4319 K  
 256 to 4254 K with  $\gamma_0 = 2.25$  for  $\gamma_\infty$  varying from 1.25 to 0.6, respectively.

257 The linear fits of the mean values of  $T_{CMB}^{is}$  yield good  $\chi^2$  values, with the parameters values  
 258 given in Table 4.  $T_{CMB}^{is}$  correlates positively with both  $\gamma_0$  and  $\gamma_\infty$ , and the strongest effect of  $\gamma_0$  is  
 259 due to the higher value of  $a_1$  (Table 4).

260 The variations in temperature are minimized if  $\gamma_0 \geq 2$  and  $\gamma_\infty \leq 1$ , as shown by the cor-  
 261 responding values of the fit in Table 4. Therefore, choosing high values of  $\gamma_0$  (like 1.837 as in  
 262 Dewaele et al. (2006) and Clesi & Deguen (2023) or 2.05 as in Kuwayama et al. (2020)) combined  
 263 with relatively low values of  $\gamma_\infty$  can minimize the error in the output. The  $\gamma_\infty$  value of 1.3 used  
 264 in Dewaele et al. (2006) and Clesi & Deguen (2023) or 1.2 for Dubrovinsky et al. (2000) are a bit  
 265 high in terms of minimizing the dispersion and error in the output.

266 Let us now assume that the values of  $\gamma_0 = 1.875$  and  $\gamma_\infty = 1.305$  in the original study of Clesi  
 267 & Deguen (2023) (taken from Dewaele et al. (2006)) are wrong. It is then possible to estimate the  
 268 error induced in the final mean temperature by calculating the variation in temperature induced  
 269 by a variation in the values of  $\gamma_0$  and  $\gamma_\infty$  using the parameters in Table 4. For  $\gamma_0 = 1.875$ , a  
 270 variation in  $\gamma_\infty$  value by 0.1 induces a variation of the temperature of  $\sim 15$  K. The main parameter  
 271 that can induce error is  $\gamma_0$ : for  $\gamma_\infty = 1.25$ , a deviation of  $\pm 0.1$  in the value of  $\gamma_0$  leads to a  
 272 deviation of  $\sim 90$  K. Then if the value of  $\gamma_0$  is not the one proposed by Dewaele et al. (2006),

273 but the one proposed by Kuwayama et al. (2020) ( $\gamma_0 = 2.05$ ), even if the value of  $\gamma_\infty$  is correct,  
274 then  $\Delta T$  would be a positive 200K, meaning that the initial value from Clesi & Deguen (2023)  
275 underestimates the temperature. Getting the value wrong would place the conclusions of the study  
276 towards a conservative estimate of the temperature.

## 277 **6 DISCUSSION**

278 We propose in the previous sections an overview of the effect of each parameter on the output of a  
279 given model. All three formalisms have their own merits and none of them should be discarded *a*  
280 *priori*. In this section we will provide an estimate of the error induced by the type and values used  
281 in each formalism, and argue that one can choose the formalism that suits the best the purpose of  
282 the study.

### 283 **6.1 Thermodynamical theory compliance vs practicality**

284 In terms of theoretical merits, Al'Tshuler et al. (1987) is the more correct formalism. It is de-  
285 rived from the study of variations in isotherms using the original definition of the parameter of  
286 Grüneisen (1912), and Mie-Grüneisen equation of state. The whole original paper of Al'Tshuler  
287 et al. (1987), is very strong in terms of theoretical compliance, since the relationship between den-  
288 sity and Grüneisen parameter is derived by calculus alone. It also takes into account the asymptotic  
289 behavior of  $\gamma$  at high pressure (Burakovsky & Preston 2004). On the other hand, the formalism of  
290 Anderson (1967) is justified only by the sentence:

291 *"Assuming the power law  $\gamma = \gamma_0 (V/V_0)^q$ "*

292 followed by an integration of the  $\gamma$  function. In term of theoretical soundness, it is less sound than  
293 Al'Tshuler et al. (1987) study. But in term of integration and data fitting, it is more convenient.  
294 Indeed, this formalism combined with a Murnaghan equation of state yield an easy-to-integrate  
295 formula, while still fitting the experimental data.

296 The same kind of reasoning applies for studies using constant  $\gamma$ , despite its limitations. Table  
297 2 shows that the variations in temperature induced by a choice of constant value are much larger.  
298 Furthermore, there is extensive experimental (Boehler & Ramakrishnan 1980; Dubrovinsky et al.

	Absolute $\Delta T$ (K)	Relative $\Delta T$ (%)
Mean	3.21	0.08
Minimum	0.008	0.0001
Maximum	8.05	0.20

**Table 5.** Difference  $\Delta T$  between the core temperature  $T_{CMB}^{is}$  obtained using Anderson’s and Al’Tshuler’s power laws with the mean values of the parameters given in Table 1. The table gives the mean difference amongst our core-formation models (Clesi & Deguen 2023), as well as the minimum and maximum of  $\Delta T$ . The formalism of Al’Tshuler is the reference point for calculating the relative variation in temperature

299 2000) and theoretical (Gilvarry 1956; Al’Tshuler et al. 1987) evidences that the Grüneisen pa-  
 300 rameter is not independent of pressure. However, the integration of a constant parameter within  
 301 a much more complicated model tends to simplify readability and interpretations. One example  
 302 is the study of the energetics of the core (*e.g.* Labrosse 2015):  $\gamma$  is not expected to vary strongly  
 303 within the core, and the effect of these variations is likely secondary compared to the effect of  
 304 thermal conductivity variations.

## 305 6.2 Assessing the uncertainties in the output of the model

306 Using the dataset of Murphy et al. (2011), we fitted the range of plausible value for each param-  
 307 eter in the formalism of Anderson (1967) and Al’Tshuler et al. (1987). This allows us to assess  
 308 the error induced by choosing one formalism over another, and the error induced by choosing a  
 309 parameter value over another in a given formalism. When using the mean value presented in Table  
 310 1 in each formalism, we can compare the effect of choosing one formalism over another by calcu-  
 311 lating, for each model in the dataset, the difference in  $T_{CMB}^{is}$ . In Table 5, we show the results of this  
 312 comparison with  $\Delta T = T_{CMB}^{is}(Anderson) - T_{CMB}^{is}(Al'Tshuler)$ . The formalism of Anderson  
 313 tends to yield higher values of  $T_{CMB}^{is}$  in any case, but the difference is small (8 K, 0.2% of varia-  
 314 tion maximum). Therefore, as long as the parameters of each formalism are consistently fitted to  
 315 the same dataset, choosing a formalism does not induce much variations. On the other hand, the  
 316 range of values chosen within a formalism is much more important than the variations induced  
 317 by a chosen formalism. In Table 6 we show the range of variation when using the maximum and  
 318 minimum values of the parameters presented in Table 1. Variation in the values of  $\gamma_0$  is the most

	Mean $\Delta T$	Minimum $\Delta T$	Maximum $\Delta T$
$\gamma_0 = 1.555$	-300 K (-7.56%)	-226 K (-5.47%)	-334 K (- 8.52%)
$\gamma_0 = 2.195$	331.5 K (8.34%)	243 K (5.90%)	372 K (9.49%)
$b = 0.432$	152 K (3.8%)	136 K (3.30%)	156 (3.98%)
$b = 1.07$	-132 K (8.34%)	-118 K (5.89%)	-136 K (9.48%)
$\gamma_0 = 1.608$	-279 K (-7.03%)	-205 K (-4.98%)	-313 K (-7.99%)
$\gamma_0 = 2.258$	311 K (7.83%)	223 K (5.43%)	351 K (8.97%)
$\gamma_\infty = 0.591$	-27.15 K (-0.68%)	-26 K (-0.64%)	-27 K (-0.70%)
$\gamma_\infty = 1.241$	47 K (1.17%)	45 K (1.09%)	47 K (1.19%)

**Table 6.** Variation of  $\Delta T$  within a chosen formalism. The absolute value are in K, the number in parenthesis are the variation relatively to the mean value in %. Top part of the Table: Anderson's power law parameter. Bottom part: Al'Tshuler power law parameter. The variation on temperature is calculated using the temperature obtained by calculating with the mean value of the parameter presented in Table 1. The terms maximum and minimum refers to the absolute deviation from the initial value, not to the value itself (i.e -205 K is a higher value than -313 K but the absolute variation is lower) .

319 important: the mean variation induced by a change in  $\gamma_0$  value in both formalisms yield a mean  
320  $\Delta T$  of  $\sim 300$  K, slightly lower in the Al'Tshuler formalism (Table 6). Varying the parameter  $\gamma_\infty$   
321 within the range given in table 1 yield a low error range, between  $-26$  K and  $+50$  K (Table 6). On  
322 the other hand, the range of  $b$  values given in Table 1 yield variations of temperature between  $-136$   
323 K and  $+156$  K. The Anderson formalism is more prone to yielding large error: taking into account  
324 both parameters value ranges, the final value of  $T_{CMB}^{is}$  can vary by  $\sim 20\%$ , with a mean variation  
325 of  $11 - 15\%$ . The range of  $T_{CMB}^{is}$  is smaller when using Al'Tshuler formalism: given the small  
326 variation induced by an error on  $\gamma_\infty$ , the maximum error on the final value of  $T_{CMB}^{is}$  is  $\sim 10\%$ ,  
327 with a mean error of  $\sim 8\%$ . In summary, the Al'Tshuler formalism yield lower uncertainties than  
328 the Anderson formalism on this type of model. However, when fitting any of the formalism to  
329 the same dataset, there is little to none variation in the output (Table 5). Since, as it is done in this  
330 study, it is possible to explain satisfactorily the same data with two different formalisms, the choice  
331 of formalism is not critical. For instance the data of Boehler & Ramakrishnan (1980) is fitted with  
332 Anderson (1967) formalism, but is used by Al'Tshuler et al. (1987) to test the formalism. The two  
333 formalisms are close in terms of mathematical writing (both of them are power laws) so it may

334 be that for a given problem and a given dataset of  $\gamma$  values, either formalism can be used (with  
335 different values of parameters). In this instance it depends on the quality of the data available and  
336 the best fit available. This problem of uncertainties range and representativity of the data needs to  
337 be addressed when choosing a formalism and the values of parameters.

### 338 **6.3 Choosing a formalism and its parameter value: a function of the study's goal**

339 In the original study of Clesi & Deguen (2023) the choice has been made to use the formalism  
340 of Al'Tshuler et al. (1987) with the values of Dewaele et al. (2006). In the supplementary infor-  
341 mation of the same study are presented different results with the Grüneisen parameter formalism  
342 of Anderson (1967) with the values of Kuwayama et al. (2020). The results are sensibly different  
343 with everything else being the equal. In this section we argue that, for this particular type of model,  
344 it is indeed better to use Al'Tshuler et al. (1987) formalism, because it enhances the robustness  
345 and replicability of the results. Indeed, using Al'Tshuler formalism is limiting the variance and  
346 the risk of error, as shown previously in Section 5, and limits the overall uncertainty of the result  
347 as shown in Section 6.2. Furthermore, in the models presented in Clesi & Deguen (2023) and  
348 briefly re-explained in section 2.1, there are several hypotheses that are made and are a source of  
349 possible error in the model; among others: the number of element in the compositional model, the  
350 equilibrium rate, the discretization of core/mantle segregation in 20 steps, the choice of equation  
351 of state, the parameters values of equation of state, the neglect of dissipation and diffusion, the  
352 thermal state of the solid mantle... All of these hypotheses are more accurately described and jus-  
353 tified in the original publication. On top of these simplifying hypotheses, the values of  $\gamma_0$  and  $\gamma_\infty$   
354 from Dewaele et al. (2006) are assumed to be independent of the composition of the core, which  
355 might be a source of error in the model. Choosing a robust formalism that limits the variation if  
356 those values are wrong is then a better option: for instance the main purpose of the publication of  
357 Clesi & Deguen (2023) is to show the existence of a correlation between core composition and its  
358 temperature, doing so by applying a number of hypotheses, which is a broader goal than getting  
359 a precise value for the core temperature. Thus, limiting the scattering of the results when many  
360 other process in the model might also be a source of scattering helps us to get a better view of the

361 problem. After all, for models of this type, it may be hard to tell if the scattering of the results is an  
362 actual scattering or an artifact created by the hypotheses and calculations techniques. This kind of  
363 limitation in the scattering also facilitates comparison between studies. For instance, one topic that  
364 is highly debated is the amount of light elements such as N, H or C in the core (Malavergne et al.  
365 2019; Grewal et al. 2019; Fischer et al. 2020; Blanchard et al. 2022; Suer et al. 2023). The pres-  
366 ence of such elements in the core will affect the temperature of the core by affecting the density of  
367 the metal, which in turn affects the temperature (through the effect of density on  $\gamma$ ; see Equations  
368 2, 7 and 8. However, each of the aforementioned study use a different model of accretion with a  
369 different set of hypothesis than in the Clesi & Deguen (2023). If one were to calculate the effect of  
370 carbon on temperature using the data and accretion models of Fischer et al. (2020) or Blanchard  
371 et al. (2022) studies in combination with a thermal evolution model, and find a significant effect of  
372 the carbon concentration on the temperature, can this effect be attributed to carbon or to the type  
373 of accretion and thermal model used to calculate carbon concentration and temperature? Among  
374 the source of uncertainties is the Grüneisen parameter formalism and value. Using a less sensitive  
375 formalism such as Al'Tshuler will at least close one of the point of discussion about the validity of  
376 the results: whether or not the values of  $\gamma_0$  and  $\gamma_\infty$  are the 'true' values, at least the error is low and  
377 if differences arise between models, then they are probably not due to the Grüneisen parameter. On  
378 the other hand, if the end goal is to best describe the entirety of the phenomenon or get a precise  
379 estimate of the core temperature (Driscoll & Davies 2023; Dobrosavljevic et al. 2022), then the  
380 best formalism is the one that fits the best the data, or the values that are calculated directly within  
381 *ab initio* studies (Vočadlo 2007; Alfè 2009; Alfè et al. 2007). If one would use a core segrega-  
382 tion model to calculate the actual temperature at the CMB instead of highlighting the correlations  
383 between parameters, or actually deriving a precise value on those correlations, then the choice of  
384 formalism and parameters value must be driven by the quality of the data, the quality of the fit,  
385 and the range of uncertainties on the parameters as highlighted in section 6.2. As an example, let  
386 us assume one wants to calculate the effect of hydrogen incorporation in the core on temperature  
387 using for instance models from Clesi et al. (2018), Malavergne et al. (2019) or Suer et al. (2023).  
388 There are some data available on the hydrogen effect on the Grüneisen parameter (Umemoto &

389 Hirose 2015). If Anderson’s formalism fitted to the data from Umemoto & Hirose (2015) yields  
 390 a narrower range of value for  $\gamma_0$  and  $b$ , than the range of value for  $\gamma_0$  and  $\gamma_\infty$  obtained through  
 391 fitting the data with Al’Tshuler formalism, then using the formalism of Anderson would be better,  
 392 especially if the range is narrow enough to yield smaller error than the one presented in Table 6.

#### 393 **6.4 Implications for the CMB temperature**

394 As highlighted in the previous sections, there are some limitations to the inferences that can be  
 395 made yet as to the relationship between the Grüneisen parameter and the core temperature. The  
 396 main goal of this study is to derive the sensitivity of  $T_{CMB}^{is}$  to the variations of parameters control-  
 397 ling the Grüneisen parameter. However, from the sensitivity study some implications can be drawn  
 398 about the initial temperature of the core.

399 All three formalisms applied to the model described in Section 2.1 can yield acceptable  $T_{CMB}^{is}$   
 400 for the Earth when compared to current estimates of CMB temperature from Zhang et al. (2016) or  
 401 Davies et al. (2015) ( $4000 \pm 200K$ ), Nomura et al. (2014) ( $3570 \pm 200K$ ) or Dobrosavljevic et al.  
 402 (2022) ( $3500 \pm 200K$ ). In all the formalisms presented, it is possible to find values of the parameters  
 403 that yield initial  $T_{CMB}^{is}$  higher than the current estimates listed above. However, none of the values  
 404 tested and presented in Figures 4, 5 and 6 can yield initial temperature at the CMB compatible  
 405 with the estimates of Andrault et al. (2017) ( $5400 \pm 100 K$ ) or Driscoll & Davies (2023) (5000 to  
 406 6000 K). This may be due to the own limitations of the model used in this study. Indeed, among  
 407 other limitations described in the original paper (Clesi & Deguen 2023), the viscous dissipation  
 408 that tends to increase temperature of the core (King & Olson 2011) is neglected, thus leading to  
 409 lower temperatures. Furthermore the choice of the Murnaghan equation of state to simplify the  
 410 calculations can also lead to an underestimation of temperature. This does show the importance of  
 411 having constraints on this parameter when trying to constrain the core temperature precisely.

## 412 **7 CONCLUSION**

413 The Grüneisen parameter  $\gamma$  is an important parameter when studying the thermal state of the core,  
 414 yet its value is not very well known for different composition of iron alloys in the core. Different

415 formalisms are used throughout the literature: constant values, *ad hoc* power law (Anderson 1967)  
416 and thermodynamically derived power law (Al'Tshuler et al. 1987). With this sensitivity study, we  
417 show that the thermodynamically derived power law of Al'Tshuler et al. (1987) is less likely to  
418 yield errors when the actual values of the parameters controlling  $\gamma$  are not precisely known, and is  
419 theoretically more sound than the *ad hoc* power law of Anderson (1967).

420 However, with the data at hand it is not yet possible to exclude any formalism or parameter  
421 values based on this study alone. Nonetheless, the sensitivity of temperature to the Grüneisen  
422 parameter can be high depending on the formalism adopted and need to be acknowledged when  
423 modeling temperature evolution. Further work in constraining the compositional dependencies of  
424 the parameters would greatly improve the thermal models of the core and their links to the light  
425 element concentrations.

## 426 **ACKNOWLEDGMENT**

427 This work was supported by the European Research Council (ERC) under the European Unions  
428 Horizon 2020 research and innovation programme (grant number 716429). ISTerre is part of Labex  
429 OSUG@2020 (ANR10 LABX56). The authors declare no other sources of funding and no com-  
430 peting interest.

## 431 **Data availability**

432 The code and data will be made available upon demand to the corresponding author.

## 433 **REFERENCES**

- 434 Alfè, D., Gillan, M., & Price, G., 2007. Temperature and composition of the earth's core, *Contemporary*  
435 *Physics*, **48**(2), 63–80.
- 436 Alfè, D., 2009. Temperature of the inner-core boundary of the Earth: Melting of iron at high pressure from  
437 first-principles coexistence simulations, *Physical Review B*, **79**(6), 060101.
- 438 Al'Tshuler, L., Brusnikin, S., & Kuz'Menkov, E., 1987. Isotherms and Grüneisen functions for 25 metals,  
439 *Journal of Applied Mechanics and Technical Physics*, **28**(1), 129–141.

- 440 Anderson, O. L., 1967. Equation for thermal expansivity in planetary interiors, *Journal of Geophysical*  
441 *Research*, **72**(14), 3661–3668.
- 442 Anderson, W. W. & Ahrens, T. J., 1994. An equation of state for liquid iron and implications for the  
443 Earth's core, *Journal of Geophysical Research: Solid Earth*, **99**(B3), 4273–4284.
- 444 Andraut, D., Bolfan-Casanova, N., Nigro, G. L., Bouhifd, M. A., Garbarino, G., & Mezouar, M., 2011.  
445 Solidus and liquidus profiles of chondritic mantle: Implication for melting of the Earth across its history,  
446 *Earth and planetary science letters*, **304**(1-2), 251–259.
- 447 Andraut, D., Bolfan-Casanova, N., Bouhifd, M., Boujibar, A., Garbarino, G., Manthilake, G., Mezouar,  
448 M., Monteux, J., Parisiades, P., & Pesce, G., 2017. Toward a coherent model for the melting behavior of  
449 the deep earth's mantle, *Physics of the Earth and Planetary Interiors*, **265**, 67–81.
- 450 Badro, J., Côté, A. S., & Brodholt, J. P., 2014. A seismologically consistent compositional model of earth's  
451 core, *Proceedings of the National Academy of Sciences*, **111**(21), 7542–7545.
- 452 Blanchard, I., Rubie, D.C., Jennings, E.S., Franchi, I.A., Zhao, X., Petitgirard, S., Miyajima, N., Jacobson,  
453 S.A. & Morbidelli, A., 2022. The metal–silicate partitioning of carbon during earth's accretion and its  
454 distribution in the early solar system, *Earth and Planetary Science Letters*, **580**, 117374.
- 455 Boehler, R. & Ramakrishnan, J., 1980. Experimental results on the pressure dependence of the grüneisen  
456 parameter: A review, *Journal of Geophysical Research: Solid Earth*, **85**(B12), 6996–7002.
- 457 Bouffard, M., Landeau, M., & Goument, A., 2020. Convective erosion of a primordial stratification atop  
458 Earth's core, *Geophysical Research Letters*, **47**(14), e2020GL087109.
- 459 Brown, J. M. & McQueen, R. G., 1986. Phase transitions, Grüneisen parameter, and elasticity for shocked  
460 iron between 77 GPa and 400 GPa, *Journal of Geophysical Research: Solid Earth*, **91**(B7), 7485–749.
- 461 Burakovsky, L. & Preston, D. L., 2004. Analytic model of the grüneisen parameter all densities, *Journal*  
462 *of Physics and Chemistry of Solids*, **65**(8-9), 1581–1587.
- 463 Clesi, V., Bouhifd, M. A., Bolfan-Casanova, N., Manthilake, G., Schiavi, F., Raepsaet, C., Bureau, H.,  
464 Khodja, H., & Andraut, D., 2018. Low hydrogen contents in the cores of terrestrial planets, *Science*  
465 *advances*, **4**(3), e1701876.
- 466 Clesi, V. & Deguen, R., 2023. Linking the core heat content to earth's accretion history, *Geochemistry,*  
467 *Geophysics, Geosystems*, **24**(5), e2022GC010661.
- 468 Davies, C., Pozzo, M., Gubbins, D. & Alfe, D., 2015. Constraints from material properties on the dynamics  
469 and evolution of Earth's core, *Nature Geoscience*, **8**(9), 678–685.
- 470 Dewaele, A., Loubeyre, P., Occelli, F., Mezouar, M., Dorogokupets, P. I., & Torrent, M., 2006. Quasi-hy-  
471 drostatic equation of state of iron above 2 Mbar, *Physical Review Letters*, **97**(21), 215504.
- 472 Dobrosavljevic, V. V., Zhang, D., Sturhahn, W., Zhao, J., Toellner, T. S., Chariton, S., Prakapenka, V. B.,  
473 Pardo, O. S., & Jackson, J. M., 2022. Melting and phase relations of fe-ni-si determined by a multi-  
474 technique approach, *Earth and Planetary Science Letters*, **584**, 117358.

- 475 Driscoll, P. & Davies, C., 2023. The “new core paradox:” challenges and potential solutions, *Journal of*  
476 *Geophysical Research: Solid Earth*, p. e2022JB025355.
- 477 Dubrovinsky, L., Saxena, S., Dubrovinskaia, N., Rekh, S., & Le Bihan, T., 2000. Grüneisen parameter of  
478  $\epsilon$ -iron up to 300 GPa from in-situ X-ray study, *American Mineralogist*, **85**(2), 386–389.
- 479 Fischer, R. A., Cottrell, E., Hauri, E., Lee, K. K., & Le Voyer, M., 2020. The carbon content of earth and  
480 its core, *Proceedings of the National Academy of Sciences*, **117**(16), 8743–8749.
- 481 Gilvarry, J. J., 1956. Grüneisen's law and the fusion curve at high pressure, *Physical Review*, **102**(2), 317.
- 482 Gomi, H., Ohta, K., Hirose, K., Labrosse, S., Caracas, R., Verstraete, M. J., & Hernlund, J. W., 2013. The  
483 high conductivity of iron and thermal evolution of the earth's core, *Physics of the Earth and Planetary*  
484 *Interiors*, **224**, 88–103.
- 485 Grewal, D.S., Dasgupta, R., Sun, C., Tsuno, K., & Costin, G., 2019. Delivery of carbon, nitrogen, and  
486 sulfur to the silicate Earth by a giant impact, *Science advances*, **5**(1), eaau3669.
- 487 Grüneisen, E., 1912. Theorie des festen zustandes einatomiger elemente, *Annalen der Physik*, **344**(12),  
488 257–306.
- 489 Hirose, K., Labrosse, S., & Hernlund, J., 2013. Composition and state of the core, *Annual Review of Earth*  
490 *and Planetary Sciences*, **41**, 657–691.
- 491 Hsieh, W.-P., Goncharov, A. F., Labrosse, S., Holtgrewe, N., Lobanov, S. S., Chuvashova, I., Deschamps,  
492 F., & Lin, J.-F., 2020. Low thermal conductivity of iron-silicon alloys at earth's core conditions with  
493 implications for the geodynamo, *Nature communications*, **11**(1), 3332.
- 494 Ichikawa, H., Tsuchiya, T. & Tange, Y., 2014. The P-V-T equation of state and thermodynamic properties  
495 of liquid iron, *Journal of Geophysical Research: Solid Earth*, **119**(1), 240–252.
- 496 Jacobson, S. A., Rubie, D. C., Hernlund, J., Morbidelli, A., & Nakajima, M., 2017. Formation, stratifica-  
497 tion, and mixing of the cores of Earth and Venus, *Earth and Planetary Science Letters*, **474**, 375–386.
- 498 Jeanloz, R., 1979. Properties of iron at high pressures and the state of the core, *Journal of Geophysical*  
499 *Research: Solid Earth*, **84**(B11), 6059–6069.
- 500 King, C. & Olson, P., 2011 Heat partitioning in metal-silicate plumes during Earth d, *Earth and Planetary*  
501 *Science Letters*, **304**(3-4), 577–586.
- 502 Kuwayama, Y., Morard, G., Nakajima, Y., Hirose, K., Baron, A. Q., Kawaguchi, S. I., Tsuchiya, T.,  
503 Ishikawa, D., Hirao, N., & Ohishi, Y., 2020. Equation of state of liquid iron under extreme conditions,  
504 *Physical Review Letters*, **124**(16), 165701.
- 505 Labrosse, S., 2015. Thermal evolution of the core with a high thermal conductivity, *Physics of the Earth*  
506 *and Planetary Interiors*, **247**, 36–55.
- 507 Landeau, M., Olson, P., Deguen, R., & Hirsh, B. H., 2016. Core merging and stratification following giant  
508 impact, *Nature Geoscience*, **9**(10), 786–789.
- 509 Landeau, M., Fournier, A., Nataf, H.-C., Cébron, D., & Schaeffer, N., 2022. Sustaining earth's magnetic

- dynamo, *Nature Reviews Earth & Environment*, **3**(4), 255–269.
- Lin, J.-F., Campbell, A. J., Heinz, D. L., & Shen, G., 2003. Static compression of iron-silicon alloys: Implications for silicon in the earth's core, *Journal of Geophysical Research: Solid Earth*, **108**(B1).
- Malavergne, V., Bureau, H., Raepsaet, C., Gaillard, F., Poncet, M., Surble, S., Sifré, D., Shcheka, S., Fourdrin, C., Deldicque, D., et al., 2019. Experimental constraints on the fate of H and C during planetary core-mantle differentiation. Implications for the Earth, *Icarus*, **321**, 473–485.
- McDonough, W. & Sun, S.-S., 1995. The composition of the Earth, *Chemical geology*, **120**(3-4), 223–253.
- McQueen, R.G., Marsh, S.P., Taylor, J.W., Fritz, J.N. & Carter, WJ, 1970. The equation of state of solids from shock wave studies, *High velocity impact phenomena*, **293**, 294–417.
- Murphy, C. A., Jackson, J. M., Sturhahn, W., & Chen, B. 2011. Grüneisen parameter of hcp-Fe to 171 GPa, *Geophysical Research Letters*, **38**(24), L24306.
- Nomura, R., Hirose, K., Uesugi, K., Ohishi, Y., Tsuchiyama, A., Miyake, A., & Ueno, Y., 2014. Low core-mantle boundary temperature inferred from the solidus of pyrolite, *Science*, **343**(6170), 522–525.
- Suer, T.-A., Jackson, C., Grewal, D. S., Dalou, C., & Lichtenberg, T., 2023. The distribution of volatile elements during rocky planet formation, *Frontiers in Earth Science*, **11**, 1159412.
- Umemoto, K. & Hirose, K., 2015. Liquid iron-hydrogen alloys at outer core conditions by first-principles calculations, *Geophysical Research Letters*, **42**(18), 7513–7520.
- Vočadlo, L., 2007. 2.05 Mineralogy of the Earth—The Earth's Core: Iron and Iron Alloys, *Treatise on Geophysics*, 91–220.
- Wagle, F. & Steinle-Neumann, G., 2019. Liquid iron equation of state to the terapascal regime from ab initio simulations, *Journal of Geophysical Research: Solid Earth*, **124**(4), 3350–3364.
- Zhang, D., Jackson, J. M., Zhao, J., Sturhahn, W., Alp, E. E., Hu, M. Y., Toellner, T. S., Murphy, C. A., & Prakapenka, V. B., 2016. Temperature of Earth's core constrained from melting of Fe and Fe<sub>0.9</sub>Ni<sub>0.1</sub> at high pressures, *Earth and Planetary Science Letters*, **447**, 72–83.